

U.S. Army Research Laboratory

SUMMER RESEARCH TECHNICAL REPORT

Integrated Thin-film Piezoelectric Traveling Wave Ultrasonic Motor

RYAN RUDY
MENTOR: RONALD G. POLCAWICH
RF & ELECTRONICS BRANCH
SENSORS AND ELECTRON DEVICES DIRECTORATE
ADELPHI, MARYLAND

| Report Documentation Page | | | Form Approved OMB No. 0704-0188 | |
|--|------------------------------------|-------------------------------------|--|---|
| Public reporting burden for the collection of information is estimated to average 1 hour per response, including the time for reviewing instructions, searching existing data sources, gathering and maintaining the data needed, and completing and reviewing the collection of information. Send comments regarding this burden estimate or any other aspect of this collection of information, including suggestions for reducing this burden, to Washington Headquarters Services, Directorate for Information Operations and Reports, 1215 Jefferson Davis Highway, Suite 1204, Arlington VA 22202-4302. Respondents should be aware that notwithstanding any other provision of law, no person shall be subject to a penalty for failing to comply with a collection of information if it does not display a currently valid OMB control number. | | | | |
| 1. REPORT DATE AUG 2011 | | 2. REPORT TYPE | | 3. DATES COVERED 00-00-2011 to 00-00-2011 |
| 4. TITLE AND SUBTITLE Integrated Thin-film Piezoelectric Traveling Wave Ultrasonic Motor | | | 5a. CONTRACT NUMBER | |
| | | | 5b. GRANT NUMBER | |
| | | | 5c. PROGRAM ELEMENT NUMBER | |
| 6. AUTHOR(S) | | | 5d. PROJECT NUMBER | |
| | | | 5e. TASK NUMBER | |
| | | | 5f. WORK UNIT NUMBER | |
| 7. PERFORMING ORGANIZATION NAME(S) AND ADDRESS(ES) Army Research Laboratory, Adelphi, MD, 20783 | | | 8. PERFORMING ORGANIZATION REPORT NUMBER | |
| 9. SPONSORING/MONITORING AGENCY NAME(S) AND ADDRESS(ES) | | | 10. SPONSOR/MONITOR'S ACRONYM(S) | |
| | | | 11. SPONSOR/MONITOR'S REPORT NUMBER(S) | |
| 12. DISTRIBUTION/AVAILABILITY STATEMENT Approved for public release; distribution unlimited | | | | |
| 13. SUPPLEMENTARY NOTES See also ADA548876 | | | | |
| 14. ABSTRACT An integrated approach to the fabrication of thin-film piezoelectric traveling wave ultrasonic motors (USMs) at the millimeter-scale is being developed for low power, high torque motors for small-scale robotics, biomedical, and sensing applications. This paper describes the realization of ultrasonic motor stators ranging in diameter from 1.3 mm using wafer-scale micro-electromechanical system (MEMS) fabrication techniques with lead zirconate titanate (PZT) thin films. Using laser Doppler vibrometry (LDV), controlled traveling waves were demonstrated in the bulk silicon elastic medium of the stator and the standing wave behavior was characterized for control purposes. Furthermore, the resonant modes of the fabricated stators were modeled using finite element models, and the experimental results agree well with this analysis. | | | | |
| 15. SUBJECT TERMS | | | | |
| 16. SECURITY CLASSIFICATION OF: | | | 17. LIMITATION OF ABSTRACT Same as Report (SAR) | 18. NUMBER OF PAGES 18 |
| a. REPORT unclassified | b. ABSTRACT unclassified | c. THIS PAGE unclassified | | |

Contents

| | |
|----------------------------------|------------|
| List of Figures | 87 |
| List of Tables | 87 |
| Abstract | 88 |
| Acknowledgments | 89 |
| Student Bio | 90 |
| 1. Introduction | 91 |
| 2. Design and Modeling | 91 |
| 3. Results and Discussion | 94 |
| 4. Conclusions | 100 |
| 5. References | 101 |

List of Figures

| | |
|--|----|
| Figure 1. Exploded view of a piezoMEMS-based USM showing the anticipated position of the stator element in the USM. | 92 |
| Figure 2. Micrograph of a fabricated 1-mm stator showing six PZT elements intended to test standing waves. The stator is anchored in the center and released from the substrate. | 92 |
| Figure 3. B_{04} mode shown from ANSYS FEA model. Analysis showed a resonance of 1.4 MHz for a 1-mm all-silicon stator disk at this resonant mode. | 93 |
| Figure 4. B_{13} mode shown from the ANSYS FEA model. Analysis predicts a resonance frequency of 3.3 MHz for a 1-mm all-silicon stator disk. | 94 |
| Figure 5. Sequence of LDV data for a 3mm diameter disk illustrating the B_{13} clockwise traveling wave for the mode shape, shown in figure 6, created by using two input 252.2-kHz sine waves separated in phase by 90° . The black square is included to help track the progression of the traveling wave. | 95 |
| Figure 6. LDV test data from an on a 2-mm disk actuated with thin-film PZT actuated at a frequency of 718.8 kHz. This shape matches the corresponding B_{13} mode. | 95 |
| Figure 7. LDV test data from standing wave in a 2-mm disk actuated with thin-film PZT actuated at a sine wave frequency of 313.9 KHz. This shape matches the predicted B_{04} mode. | 96 |
| Figure 8. Frequency response of a 3-mm-diameter disk up to 1 MHz, illustrating numerous resonance peaks, including the highlighted B_{13} mode. | 96 |
| Figure 9. Maximum displacement for different electrodes, frequencies, and excitation voltages shows the amplitude is significantly affected by both the voltage and excitation frequency. | 97 |
| Figure 10. Maximum deflection as a function of applied voltage shows a significant cubic contribution to the response. | 98 |
| Figure 11. Frequency response of the stator to a square wave input at the resonance frequency displays no significant high frequency components. | 99 |
| Figure 12. B_{13} mode shape in a 3-mm-diameter disk from square wave actuation at the resonance frequency shows that a square waveform does not significantly affect the mode shape. | 99 |

List of Tables

| | |
|---|----|
| Table 1. Example of modeled motor parameters. | 93 |
| Table 2. Calculated Q-factor for various conditions. | 98 |

Abstract

An integrated approach to the fabrication of thin-film piezoelectric traveling wave ultrasonic motors (USMs) at the millimeter-scale is being developed for low power, high torque motors for small-scale robotics, biomedical, and sensing applications. This paper describes the realization of ultrasonic motor stators ranging in diameter from 1–3 mm using wafer-scale micro-electromechanical system (MEMS) fabrication techniques with lead zirconate titanate (PZT) thin films. Using laser Doppler vibrometry (LDV), controlled traveling waves were demonstrated in the bulk silicon elastic medium of the stator and the standing wave behavior was characterized for control purposes. Furthermore, the resonant modes of the fabricated stators were modeled using finite element models, and the experimental results agree well with this analysis.

Acknowledgments

I wish to acknowledge the mentorship of Gabe L. Smith and Ronald G. Polcawich, and the assistance in device fabrication by Luz Sanchez, Brian Power, and Joel Martin.

Student Bio

I am currently attending the University of Maryland – College Park and am sponsored by the Science, Mathematics & Research for Transformation (SMART) fellowship program. I have just finished my first year in a Ph.D. program. I received both my bachelor's (2009) and master's degrees (2010) from the University of Michigan. My area of study is mechanical engineering with a focus on micro-electromechanical systems. I have previous research experience in ground mobile millimeter-scale robotics. After completion of my degree, I will work at the U.S. Army Research Laboratory.

1. Introduction

While a number of commercial traveling wave ultrasonic motors (USMs) have been demonstrated at the centimeter and larger scale, effective USMs at the millimeter (mm)-scale and below have eluded researchers (1). Rotary USMs have many advantages over electrostatic or electromagnetic motors in that they have excellent high torque, low speed performance; zero power off state with high holding torque; high efficiency; and small size (2). Rotary USMs can be created using either standing waves or traveling waves. Standing wave USMs use the vertical vibration of an inclined beam to push the rotor when the beam bends. Traveling wave USMs, first reported by Sashida in 1983 (3), use the horizontal motion of the surface of the stator to move the rotor.

Traveling wave USMs are desirable over standing wave USMs due to bidirectional actuation capabilities. Previous efforts in this area have involved the assembly of bulk-fabricated piezoelectric components, with insufficient precision to maintain and control the desired traveling waves. Flynn et al. (5) demonstrated an assembled USM using bulk ceramic lead zirconate titanate (PZT) as the actuator with an 8-mm diameter (4) and thin-film USMs as small as 5 mm. However, the thin-film devices were unable to provide bidirectional motion control, presumably due to the device configuration that prevented a well-defined traveling wave within the device. Recently, a surface micromachined ultrasonic motor, driven by a bonded bulk piezoelectric, has been reported by Kaajakari et al. (6). This device demonstrated clockwise and counterclockwise rotation while also allowing for easy integration of surface micromachined components; however, the traditional ultrasonic motor benefits of no gearing and high holding torque cannot be realized with this actuation scheme.

In the present work, we are exploiting high quality PZT thin-film materials to enable wafer-level batch fabrication with photolithographic patterning to improve manufacturing precision and reduce cost. Using wafer-scale micro-electromechanical system (MEMS) fabrication techniques with thin-film PZT on silicon-on-insulator (SOI) processing, USM stators ranging in diameter from 1–3 mm have been successfully realized.

2. Design and Modeling

The motor design leverages an integrated fabrication process using a combination of surface and bulk micromachining. Figure 1 shows an exploded view of the conceptual design, displaying the rotor, stator, and other motor components. Figure 2 shows the details of a fabricated stator.

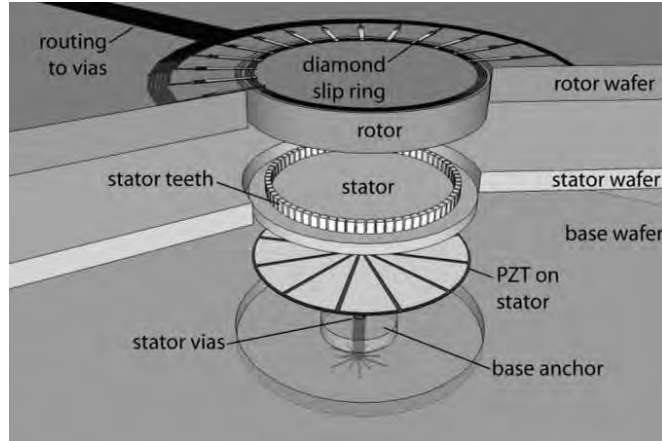


Figure 1. Exploded view of a piezoMEMS-based USM showing the anticipated position of the stator element in the USM.

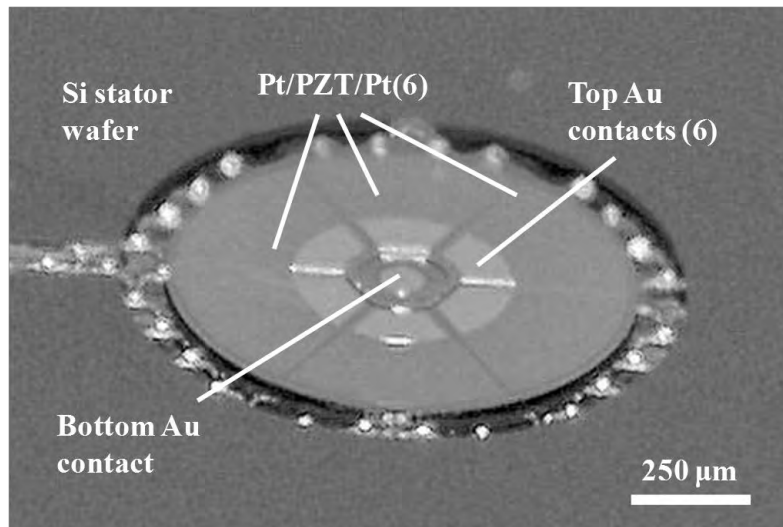


Figure 2. Micrograph of a fabricated 1-mm stator showing six PZT elements intended to test standing waves. The stator is anchored in the center and released from the substrate.

Because the demonstrated fabrication process takes advantage of photolithographic patterning and alignment for all of the components, it does not suffer from the constraints inherent to macro-scale assembly that have traditionally limited the minimum USM dimensions. The fabrication process flow for the stators uses chemical solution deposited PZT, metal sputtering and evaporation, reactive ion etching, etching via vapor hydrofluoric acid (HF), metal liftoff, ion milling, and atomic layer deposition of aluminum oxide (Al_2O_3) (9).

In order to predict the response of the USM stators, both equivalent circuit modeling and ANSYS Finite Element Analysis (FEA) modal analysis were performed. Since traveling wave motors operate through a set of complex electromechanical phenomena, an optimal design of the proposed μUSM will require an effective model to guide the design process. While various

vibration modes are under consideration for future USM motors, the B_{13} mode, consisting of 1 nodal circle and 3 nodal diameters, is being explored first. For this case, the stator is patterned with 12 conductive regions grouped into four sets of three alternating electrodes. To estimate the performance of our initial motor design, an equivalent circuit model was constructed assuming a conservative mechanical quality factor of 100. Performance estimates for this early design are shown in table 1.

Table 1. Example of modeled motor parameters.

| Parameter | Value |
|---------------------------------|--------------------|
| Voltage input | ± 1.8 V |
| Stator diameter | 1 mm |
| Stator height (without teeth) | 40 μm |
| Stator tooth height | 30 μm |
| PZT thickness | 0.25 μm |
| Eigenfrequency (B_{13} mode) | 3.4 MHz |
| Max output speed | 8.1 Hz |
| Maximum output (stall) torque | 0.14 N mm |
| Input power at 1 Hz | 3.7 mW |

ANSYS FEA modeling was used to determine modal frequencies of the standing waves. Of primary interest were the B_{03} , B_{04} , B_{13} and B_{14} modes consisting of 0 and 1 circumferential nodes and 3 and 4 nodal diameters, respectively. Figures 3 and 4 show finite element simulations of two of these mode shapes.

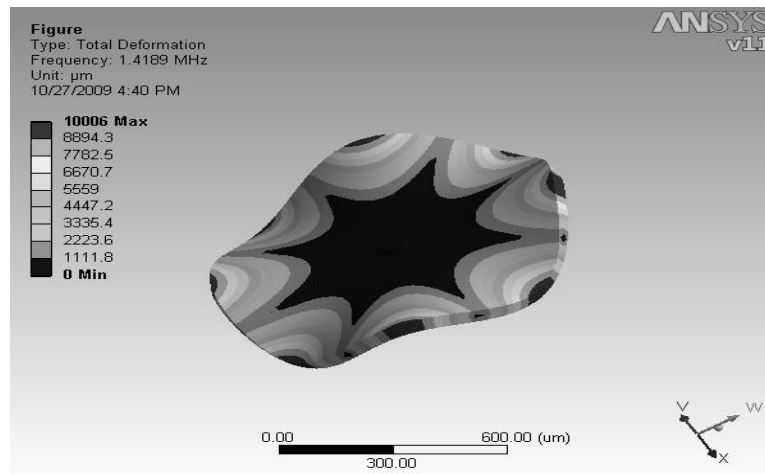


Figure 3. B_{04} mode shown from ANSYS FEA model. Analysis showed a resonance of 1.4 MHz for a 1-mm all-silicon stator disk at this resonant mode.

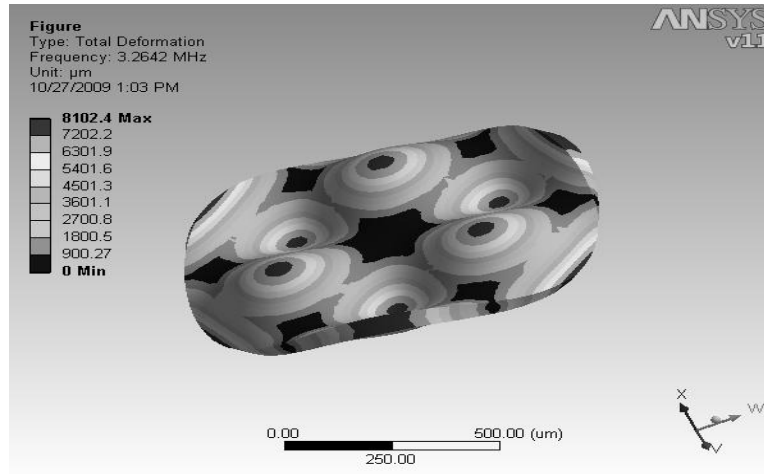


Figure 4. B_{13} mode shown from the ANSYS FEA model. Analysis predicts a resonance frequency of 3.3 MHz for a 1-mm all-silicon stator disk.

These modes are desirable as they ensure rotor stability by maintaining at least three contact points of the stator to rotor, maximize vertical displacement compared to higher order modes, and minimize the required number of actuation regions.

3. Results and Discussion

A controlled traveling wave was induced in the fabricated stators using two out-of-phase input waveforms. This controlled traveling wave, which can be driven in either a clockwise or counterclockwise direction, allows the motor to operate in both directions as opposed to the standing wave rotary USMs reported in reference 10. Figure 5 illustrates the traveling wave using phase-stepped laser Doppler vibrometry (LDV) data. This representation illustrates the deformation of the stator over a single cycle in time, equivalent to $4 \mu\text{s}$, resulting in the wave progressing approximately 120° around the disk.

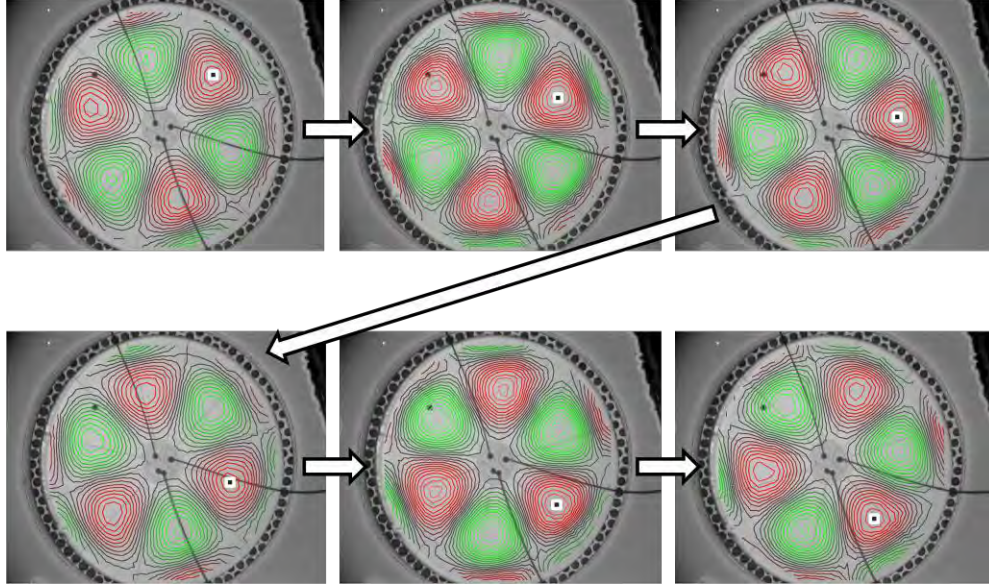


Figure 5. Sequence of LDV data for a 3mm diameter disk illustrating the B_{13} clockwise traveling wave for the mode shape, shown in figure 6, created by using two input 252.2-kHz sine waves separated in phase by 90° . The black square is included to help track the progression of the traveling wave.

The traveling waves were generated by exciting standing waves in phase and apart in space according to the identity,

$$\cos(n\theta) \cos(\omega t) + \sin(n\theta) \sin(\omega t) = \cos(n\theta - \omega t). \quad (1)$$

To characterize the standing waves, individual electrodes were used to excite the resonance mode shapes within the stators. LDV was then used to determine the mode shapes present. The resonance mode shapes for the B_{04} and B_{13} modes, shown in figures 6 and 7, match the mode shapes determined by FEA in figures 3 and 4.

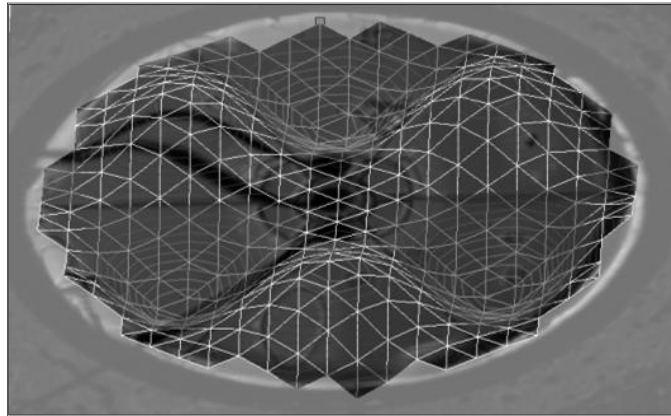


Figure 6. LDV test data from an on a 2-mm disk actuated with thin-film PZT actuated at a frequency of 718.8 kHz. This shape matches the corresponding B_{13} mode.

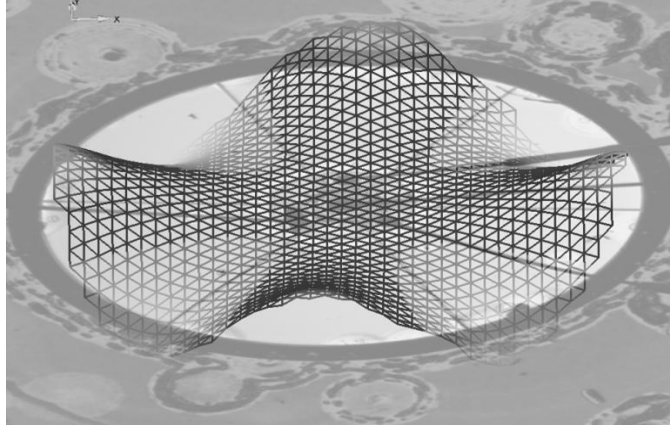


Figure 7. LDV test data from standing wave in a 2-mm disk actuated with thin-film PZT actuated at a sine wave frequency of 313.9 KHz. This shape matches the predicted B_{04} mode.

Experimental determination of the resonance frequencies was determined by inputting a 0–5 V white noise signal, using a waveform generator, and measuring the response using LDV. A Fourier transform was performed on this data to determine the frequencies of greatest amplitude. These frequencies were then isolated and examined to determine the mode shape present at each resonance frequency. Figure 8 shows the frequency response of a 3-mm-diameter disk up to 1 MHz, suggesting a number of resonances.

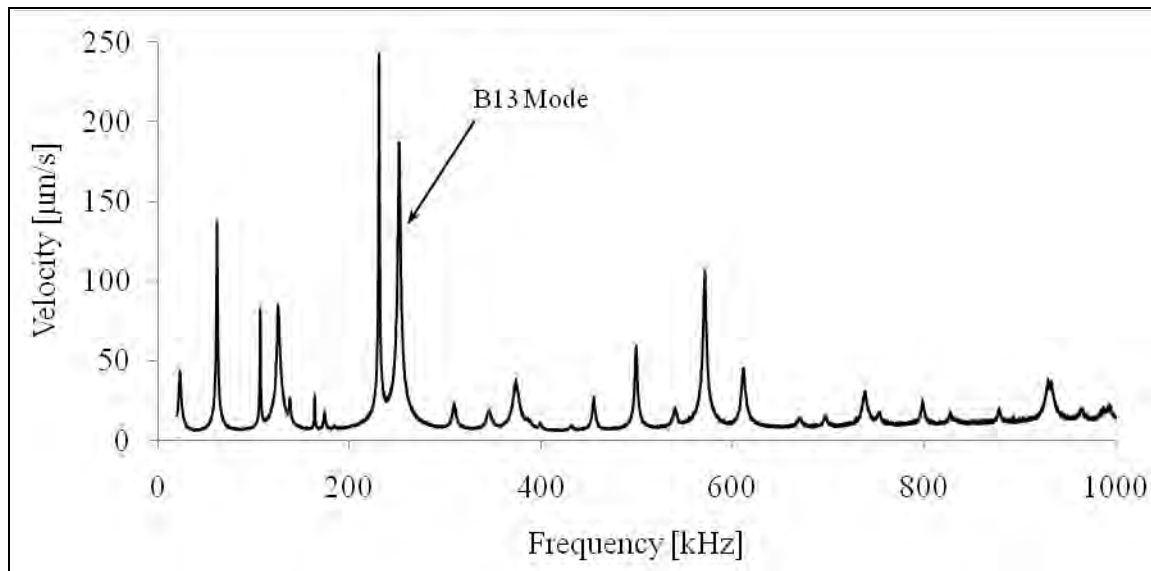


Figure 8. Frequency response of a 3-mm-diameter disk up to 1 MHz, illustrating numerous resonance peaks, including the highlighted B_{13} mode.

The desired B_{13} mode was further characterized for the effects of frequency and voltage on the deflection of the surface. To accomplish this, sinusoids of single frequencies were input to one electrode on the stator and the displacement was determined by LDV. The results of this characterization are shown in figure 9. From this plot it is clear that frequency and voltage both significantly affect the response.

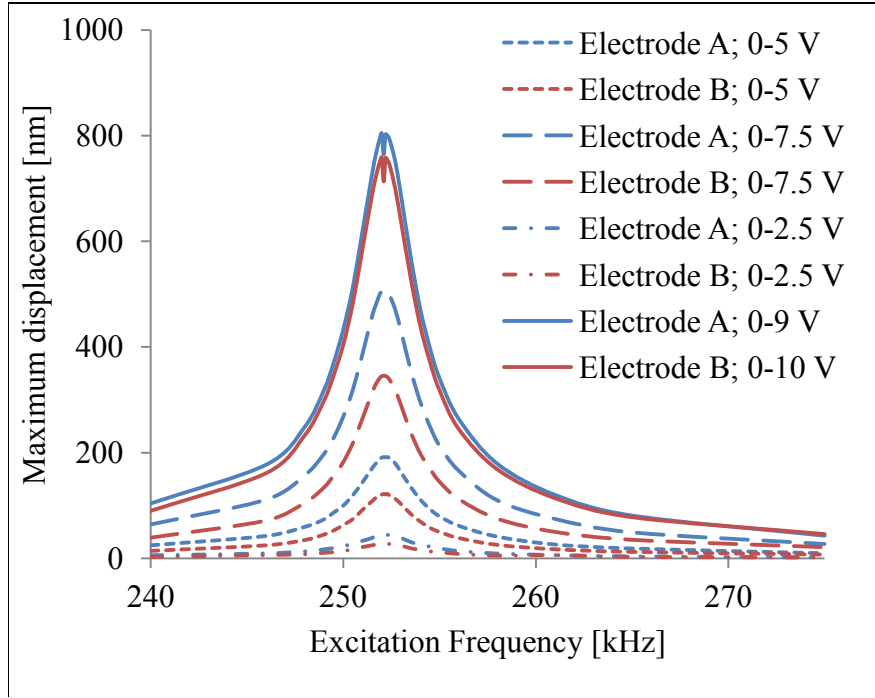


Figure 9. Maximum displacement for different electrodes, frequencies, and excitation voltages shows the amplitude is significantly affected by both the voltage and excitation frequency.

Beyond the simple qualitative conclusion that voltage and frequency affect amplitude, one can note specifics about the system. First, it is an easy extrapolation to approximate the Q-factor:

$$Q = \frac{f_p}{\Delta f}, \quad (2)$$

where f_p is the peak frequency and Δf is the bandwidth, defined as the difference between the upper and lower frequency, where the response reaches half of the maximum amplitude. Performing these calculations for each of the electrodes and voltages gives the Q-factors as recorded in table 2.

Table 2. Calculated Q-factor for various conditions.

| Condition | Q-factor |
|----------------------|----------|
| Electrode A; 0–1 V | 50.6 |
| Electrode A; 0–2.5 V | 53.9 |
| Electrode A; 0–5 V | 54.9 |
| Electrode A; 0–7.5 V | 54.6 |
| Electrode A; 0–9 V | 54.1 |
| Electrode B; 0–1 V | 55.9 |
| Electrode B; 0–2.5 V | 57.2 |
| Electrode B; 0–5 V | 56.8 |
| Electrode B; 0–7.5 V | 54.6 |
| Electrode B; 0–10 V | 54.9 |

From this, we can see that for the 3-mm-diameter stator all conditions display a Q-factor near 50. For large Q-factors, Q can be approximated:

$$Q = \frac{1}{2\zeta}. \quad (3)$$

Under this approximation, the evidence suggests that damping in the stator system is not related to displacement magnitude. From this, it can be posited that squeeze film damping, which is highly related to vibration amplitude, is not active in the analyzed stator system. Another point that can be made from the data is that the relationship between voltage and maximum displacement is cubic in nature. The points tested and the equations for the two electrodes tested are shown on figure 10. The nonlinearity is quite strong, accounting for over 60% of the calculated displacement at just a 5-V actuation. In evaluating the equations in figure 10, it is assumed that the displacement relationships should be point symmetric about this origin, thus only allowing odd functions.

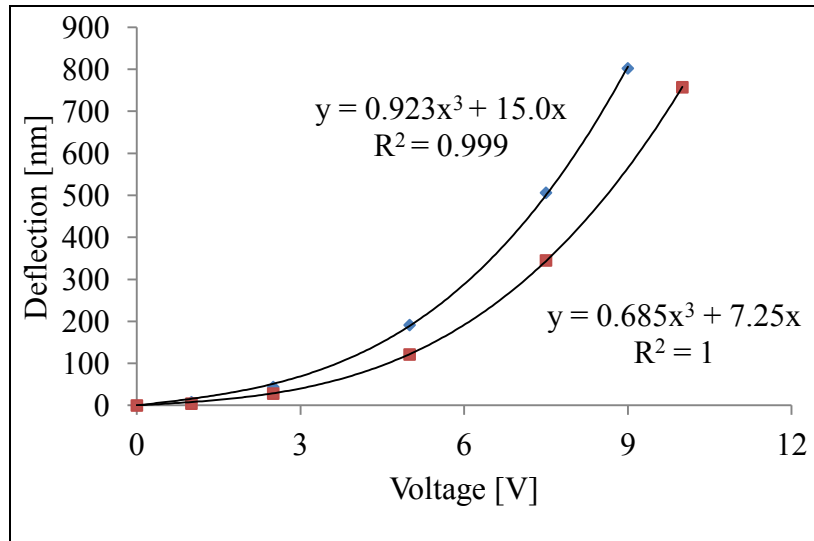


Figure 10. Maximum deflection as a function of applied voltage shows a significant cubic contribution to the response.

This sort of nonlinearity, specifically, a softening cubic nonlinearity, has been observed by others, such as Sattel (11). The nonlinear catastrophic jump phenomenon described by Sattel (11) was not observed, however. This could be due to the relatively small amplitudes of displacement; however, definitively proving this would require further investigation.

Beyond characterization of stator deflection based on sinusoidal inputs, the stators were also actuated using square waves. No significant high frequency components were observed in the frequency response, as shown in figure 11.

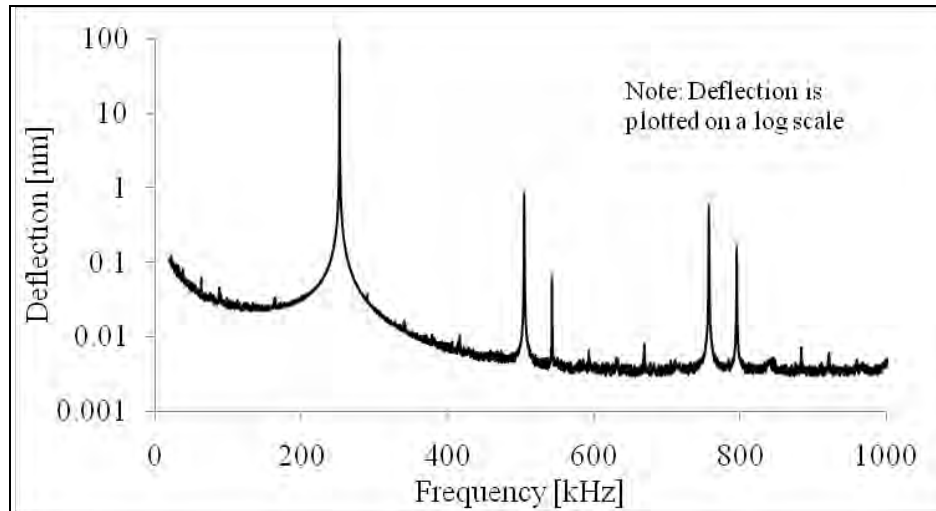


Figure 11. Frequency response of the stator to a square wave input at the resonance frequency displays no significant high frequency components.

From square wave excitation, both traveling and standing waves were induced in the stator. A standing wave from square wave excitation is shown in figure 12, illustrating the B_{13} mode shape unchanged by substituting a square wave for the sinusoidal input waveform.

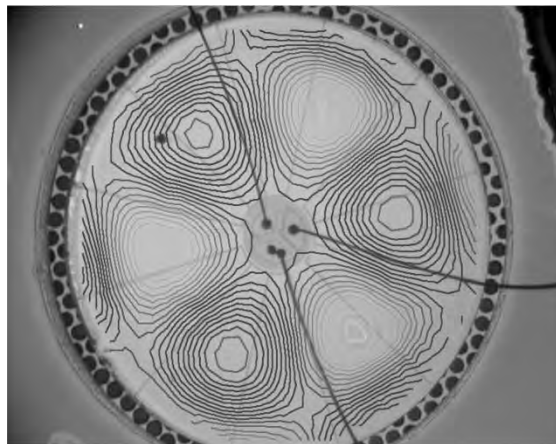


Figure 12. B_{13} mode shape in a 3-mm-diameter disk from square wave actuation at the resonance frequency shows that a square waveform does not significantly affect the mode shape.

4. Conclusions

Both standing wave and traveling wave actuation of the bulk silicon elastic medium of a microfabricated USM stator have been successfully achieved using thin-film PZT. The resonant modes of the fabricated stators have been modeled with FEA, with experimental results agreeing well with these simulations, and an analytic model to predict performance characteristics of the motors has been developed. Demonstration of square wave operation without significant high frequency components allows for the use of on-off switching rather than sinusoidal input signals. This makes integration into a portable, untethered system significantly easier. With the excellent predicted performance metrics for the microfabricated USMs and the experimental results from stator testing, the devices are expected to open the door to new opportunities for integrating miniature rotary actuation into a wide range of commercial and military applications.

5. References

1. Uchino, K.; Giniewicz, J. R. *Micromechatronics* **2003**, 417–430.
2. Uchino, K. Piezoelectric Ultrasonic Motors: Overview. *Smart Material Structures* **1998**, 7, 273–285.
3. Sashida, T. Approach of the Development for the Ultrasonic Motor. *Mechanical Automation Japan* **1983**, 15 (12), 31–35.
4. Flynn, A. M. Performance of Ultrasonic Mini-motors Using Design of Experiments. *Smart Material Structures* **1998**, 7, 286–294.
5. Flynn, A. M. et al. Piezoelectric Micromotors for Microrobots. *Journal of Microelectromechanical Systems* **March 1992**, 1 (1), 44–51.
6. Kaajakari, V.; Lal, A. Micromachined Ultrasonic Motor Based on Parametric Polycrystalline Silicon Plate Excitation. *Sensors and Actuators A: Physical* **June 2007**, 137 (1), 120–128.
7. Bronson, J. et al. Thin Film PZT Flapping Wing Actuators for Insect-Inspired Robotics. *22nd IEEE International Conference on MEMS*, Sorrento, Italy, Jan 2009.
8. Pulskamp, J. S. et al. Two Degree of Freedom PZT MEMS Actuated Flapping Wings with Integrated Force Sensing. *Hilton Head Workshop*, June 2010.
9. Smith, G. L. et al. Atomic Layer Deposited Alumina for Use as an Etch Barrier Against Xenon Difluoride Etching. *Solid-State Sensors, Actuators, and Microsystems Workshop*, Hilton Head, SC, June 2010.
10. Sashida, T. Trial Construction and Operation of an Ultrasonic Vibration Driven Motor. *Oyo Butsuri* **1982**, 51, 713–720.
11. Sattel, T. Dynamics of Ultrasonic Motors, Doctoral Thesis, Technische Universität Darmstadt, Germany, 2002.